

A low-PAPR Pilot Design and Optimization for OTFS Modulation

Davide Bergamasco, Federico Clazzer, Andrea Munari, and Paolo Casari

Abstract—Orthogonal time frequency space (OTFS) modulation has been proposed recently as a new waveform in the context of doubly-selective multi-path channels. This article proposes a novel pilot design that improves OTFS’s spectral efficiency (SE) while reducing its peak-to-average power ratio (PAPR). Instead of adopting an embedded data-orthogonal pilot for channel estimation, our scheme relies on Chu sequences superimposed to data symbols. We optimize the construction by investigating the best energy split between pilot and data symbols. Two equalizers, and an iterative channel estimation and equalization procedure are considered. We present extensive numerical results of relevant performance metrics, including the normalized mean squared error of the estimator, bit error rate, PAPR and SE. Our results show that, while the embedded pilot scheme estimates the channel more accurately, our approach yields a better tradeoff by achieving much higher spectral efficiency and lower PAPR.

I. INTRODUCTION

In the context of broadband communication systems, high-mobility wireless channels introduce severe distortions to transmitted signals by spreading their power across the time and the frequency domains. In these scenarios, orthogonal time frequency space (OTFS) modulation [1] has recently attracted a lot of attention thanks to its capability to exploit the appealing properties offered by the delay-Doppler (DD) representation of the channel. OTFS can be seen as a digital multi-carrier system that orthogonally multiplexes MN information symbols, with $M, N \in \mathbb{N} \setminus \{0\}$, in the DD domain. Any non-trivial multi-path channel destroys this orthogonality at the receiver, introducing the need for equalization to cancel the inter-carrier interference (ICI) and restore the transmitted data. One unique property of OTFS is that, when properly designed, the interaction between any of the MN sub-carriers and the channel is the same. More formally, when the *crystallization condition* [2] is fulfilled, successive replicas of the channel response in the DD domain are guaranteed to be free of aliasing. Hence, under this condition, it is sufficient to estimate the channel behavior once for all sub-carriers.

Along this line, many channel estimation algorithms have been proposed in recent years, e.g., [3]–[8]. In [3], a design

D. Bergamasco, F. Clazzer and A. Munari are with the Inst. of Communications and Navigation, German Aerospace Center (DLR), Wessling, Germany (e-mail: {davide.bergamasco, federico.clazzer, andrea.munari}@dlr.de).

P. Casari is with DISI, University of Trento, Italy (e-mail: paolo.casari@unitn.it). D. Bergamasco is also with DISI.

D. Bergamasco, F. Clazzer and A. Munari acknowledge the financial support by the Federal Ministry of Education and Research of Germany in the programme of “Souverän. Digital. Vernetzt.” Joint project 6G-RIC, project identification number: 16KISK022. The work of P. Casari was partially supported by the European Union – Next Generation EU – PNRR, Mission 4 Component 2, Investment 1.3 – PE RESTART Spoke 6 - Project EMBRACE (PE00000001, CUP E63C22002070006).

considering one single pilot allocated within an OTFS frame is considered. A sufficient guard band of empty symbols surrounds the pilot so that, even after propagating through the channel, the received pilot signal remains free of interference from data. In [4], the design is extended to multiple-input multiple-output (MIMO) channels, and in [5] a sparse Bayesian recovery is introduced to estimate the channel paths. These approaches preserve data-pilot orthogonality at the receiver, favoring accurate channel estimation and thus enabling effective data equalization. However, reserving resources for pilot and guard symbols in the OTFS frame reduces the spectral efficiency (SE) of the scheme. To improve this metric, a different design strategy that embraces data-pilot interference has also been explored. This idea has been firstly presented in the context of OTFS in [6], where a bi-dimensional pilot sequence is superimposed to data symbols so that both contributions cover one entire OTFS frame. A related construction has been proposed in [7], where a single pilot is placed within an OTFS frame full of data symbols. In [8], instead, the pilot sequence only covers one of the columns along the delay dimension of the OTFS frame, while the data is still allowed to span the entire frame.

Motivated by use cases with tight link budgets and limited energy resources, such as in satellite-enabled Internet of Things (IoT) applications, we aim to devise an OTFS scheme with low peak-to-average power ratio (PAPR) and high SE. Thus, we focus on a construction that overlaps pilots and data. Observing that a pilot sequence covering one entire column of the OTFS frame minimizes the pilot contribution to the PAPR, we proceed along the same line as [8]. However, unlike [8], we optimize the energy split among data and pilots and do not consider the number of multi-path channel components to be known. Additionally, we propose the use of Chu sequences [9], which are specifically suited to channel estimation via sparse recovery algorithms. Moreover, we present an iterative channel estimation and equalization procedure that considerably boosts the performance of non-orthogonal designs. Finally, we numerically evaluate the performance of the proposed approach in terms of the normalized mean squared error (NMSE) of the estimator, bit error rate (BER), PAPR, and SE. We compute these metrics also for an orthogonal data-pilot design and discuss the involved trade-offs together with the role of orthogonality.

II. SYSTEM MODEL

In this section, we describe the OTFS communication model, as shown in Fig. 1.



Fig. 1. IDZT-OTFS communication pipeline.

A. Transmitter

The input signal $\mathbf{X} \in \mathbb{C}^{M \times N}$ consists of MN complex symbols that represent the available degrees of freedom at the input of the communication chain. These are used to transmit data and pilot within each frame, where the two contributions are respectively contained in the matrices \mathbf{X}_d and \mathbf{X}_p so that $\mathbf{X} = \mathbf{X}_d + \mathbf{X}_p$. The signal \mathbf{X} is represented in the DD domain and, by means of the inverse discrete Zak transform (IDZT), it can be converted into its discrete-time representation $\mathbf{s} \in \mathbb{C}^{NM \times 1}$ as

$$s[t] = s[\ell + nM] = \frac{1}{\sqrt{N}} \sum_{k=0}^{N-1} \mathbf{X}[\ell, k] e^{j \frac{2\pi}{N} nk} \quad (1)$$

with $\ell \in \{0, \dots, M-1\}$, $n \in \{0, \dots, N-1\}$ and $t = \ell + nM$. The transformation shown in (1) is performed through the IDZT-block depicted in Fig. 1 and can be equivalently computed as

$$\mathbf{s} = \text{IDZT}\{\mathbf{X}\} = \text{vec}(\mathbf{X}\mathbf{F}_N^H) = (\mathbf{F}_N^H \otimes \mathbf{I}_M)\mathbf{x} \quad (2)$$

where $\mathbf{x} = \text{vec}(\mathbf{X})$, is obtained by stacking all columns of \mathbf{X} , \mathbf{F}_N is the discrete Fourier transform (DFT) matrix of size N and \otimes represents the Kronecker product. To avoid inter-frame interference, we make use of a cyclic prefix (CP) at the frame level, leading to the so-called reduced cyclic prefix (RCP) version of OTFS [10]. This is implemented by copying and pre-pending the last L samples of \mathbf{s} so that the overall signal is composed of $MN + L$ symbols. The frame duration is given as $T_f = (MN + L)T_s$, where T_s is the symbol time. Finally, the resulting digital signal is converted to the baseband continuous signal $s(t)$, up-converted to radio frequency, and transmitted over the channel. We assume the use of rectangular pulse-shaping waveforms.

B. Channel

We consider a P -sparse multi-path channel with additive white Gaussian noise (AWGN). Each propagation component has its own complex gain, propagation delay and Doppler shift represented by h_i , τ_i and ν_i respectively, for $i \in \{1, \dots, P\}$.¹ The input-output relation in the time domain is given as

$$r(t) = \sum_{i=1}^P h_i e^{j2\pi\nu_i(t-\tau_i)} s(t-\tau_i) + n(t) \quad (3)$$

¹These parameters are assumed to be constant for one frame duration as commonly done in OTFS literature. This can be explained since the DD domain requires substantial change of moving speed or propagation delays to change its representation.

where $n(t) \sim \mathcal{CN}(0, \sigma^2)$ is AWGN noise. The quantities ν_i and τ_i are expressed as a function of the delay and Doppler resolutions of the system

$$\tau_i = \ell_i \cdot T_s \quad \text{and} \quad \nu_i = \frac{k_i}{T_f} = \frac{k_i}{NMT_s}. \quad (4)$$

The delay spread and maximum Doppler shift are represented as $\ell_M = \max_{1 \leq i \leq P} (\ell_i)$ and $k_M = \max_{1 \leq i \leq P} (|k_i|)$. Using the sampling theorem it is possible to represent the band-limited signal $s(t)$ in terms of its samples [11] and by combining (3) and (4) we get, after minor manipulations

$$r[t] = \sum_{\ell=0}^{M-1} s[t-\ell] \sum_{i=1}^P h_i e^{j \frac{2\pi}{NM} k_i (t-\ell_i)} \cdot \text{sinc}(t-\ell_i) + n[t] \quad (5)$$

where $\text{sinc}(x) = \sin(\pi x)/(\pi x)$ and $\text{sinc}(0) = 1$. By assuming that $\ell_i \in \mathbb{N}$ and $k_i \in \mathbb{Z}$, meaning that τ_i and ν_i are integer multiples of the delay and Doppler resolutions, respectively, (5) can be simplified as

$$r[t] = \sum_{i=1}^P h_i e^{j \frac{2\pi}{NM} k_i (t-\ell_i)} \cdot s[t-\ell_i] + n[t]. \quad (6)$$

We can now represent the input-output relation in matrix form as [10, Section. 3]

$$\mathbf{r} = \mathbf{G}\mathbf{s} + \mathbf{n} \quad (7)$$

where the time-domain channel matrix $\mathbf{G} \in \mathbb{C}^{NM \times NM}$ is

$$\mathbf{G} = \sum_{i=1}^P h_i e^{-j \frac{2\pi}{NM} k_i \ell_i} \mathbf{\Delta}^{k_i} \mathbf{\Pi}^{\ell_i}$$

with $\mathbf{\Delta}^{k_i} = \text{diag}[e^{j \frac{2\pi}{NM} k_i \cdot (0)}, \dots, e^{j \frac{2\pi}{NM} k_i \cdot (NM-1)}]$, and where $\mathbf{\Pi}$ is the cyclic shift matrix of size $NM \times NM$

$$\mathbf{\Pi} = \begin{bmatrix} 0 & \dots & 0 & 1 \\ 1 & \dots & 0 & 0 \\ \vdots & \ddots & \vdots & \vdots \\ 0 & \dots & 1 & 0 \end{bmatrix}.$$

C. Receiver

The continuous-time signal $r(t)$ at the output of the channel is converted to baseband and sampled at frequency $f_c = \frac{1}{T_s}$ using an analog-to-digital converter (ADC). After CP removal and through the discrete Zak transform (DZT)-block, the receiver represents the signal \mathbf{r} in the DD domain as

$$\mathbf{Y} = \text{DZT}\{\mathbf{r}\} = \mathbf{F}_N \text{vec}_{MN}^{-1}(\mathbf{r})$$

where $\text{vec}_{ij}^{-1}(\mathbf{x})$ reshapes a vector of length ij into a matrix of size $i \times j$. By vectorizing the matrix \mathbf{Y} column-wise we define the vector

$$\mathbf{y} = \text{vec}(\mathbf{Y}) = (\mathbf{F}_N \otimes \mathbf{I}_M)\mathbf{r}. \quad (8)$$

Considering (7) we multiply both sides of the equality by $\mathbf{F}_N \otimes \mathbf{I}_M$. Then, by combining the obtained result with (2) and (8), we obtain the vectorized DD input-output relation

$$\mathbf{y} = \mathbf{H}\mathbf{x} + \mathbf{w} \quad (9)$$

where the DD channel matrix $\mathbf{H} \in \mathbb{C}^{NM \times NM}$ is given as

$$\mathbf{H} = (\mathbf{F}_N \otimes \mathbf{I}_M) \mathbf{G} (\mathbf{F}_N^H \otimes \mathbf{I}_M) \quad (10)$$

and $\mathbf{w} = (\mathbf{F}_N \otimes \mathbf{I}_M) \mathbf{n} \in \mathbb{C}^{NM \times 1}$ represents the noise contribution in the transformed domain.

III. PILOT DESIGN AND ESTIMATION PROCEDURE

To minimize the overhead of the pilot in terms of DD resources, a superimposed data-pilot configuration is considered. One important metric that drives our pilot signal construction is the PAPR

$$\text{PAPR}(f[t]) = \frac{\max(|f[t]|^2)}{\mathbb{E}\{f[t]\}}.$$

This quantity provides a measure of how much the envelope of a signal $f[t]$ has uneven power peaks. Ideally, we would like to find the arrangement of pilot symbols in DD domain that leads to a constant-power time signal. The IDZT modulator performs row-wise inverse fast Fourier transform (IFFT) of length N , thus recombining the energy contained in each row of \mathbf{X} . A possible pilot construction to minimize the PAPR is to equally spread the pilot energy among all the rows of \mathbf{X} [12]. This can be done by considering a pilot sequence composed of M equal-power symbols placed on a single column of \mathbf{X} , thus spanning the entire delay dimension.

A construction of this type was considered in [8] where the authors make use of Zadoff-Chu (ZC) sequences [13]. These sequences are well suited for channel estimation from a PAPR point of view given that all elements have the same amplitude. Moreover, they also have perfect periodic autocorrelation, which is equal to zero for any non-zero cyclic shift. This last property will be leveraged during the channel estimation phase to avoid pilot self-interference. When the former two properties are simultaneously met, the sequence is said to be constant amplitude zero autocorrelation (CAZAC).

One downside of ZC sequences is that the perfect autocorrelation property is only fulfilled for prime-valued lengths of the sequence. This places an additional requirement on the parameter M that represents the number of rows of the matrix \mathbf{X} , and affects several other aspects of the communication system. For example, in order to fulfill the *crystallization condition* we have to ensure that $\ell_M < M$ and $2k_M + 1 \leq N$. The dimensions of the DD matrix cannot be independently selected since their product, namely NM , represents the number of orthogonal sub-carriers inside each OTFS frame, which is equal to $(T_f - LT_s)B$ where $B = \frac{1}{T_s}$. Overall, by fixing the time-frequency resources allocated for the transmission of a frame, and thus defining its duration and bandwidth, the quantity MN becomes fixed. At this point, any choice on the selection of M implies the selection of N and vice versa. Ideally, we would like to have $N = 2^i$ with $i \in \mathbb{N}$ so that the

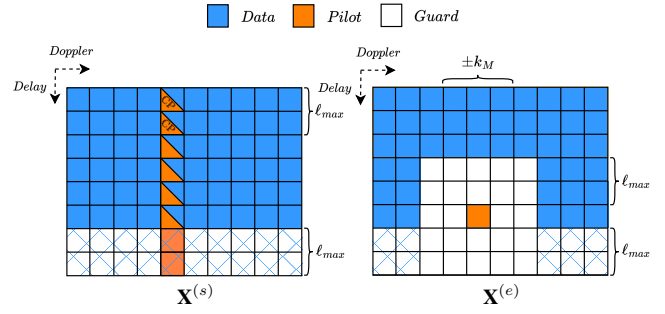


Fig. 2. Our proposed SID data-pilot design (left) vs the embedded pilot construction from [3] (right). The shaded elements represent data frame locations that would not affect the channel estimation procedure but are kept empty to enable the use of simpler equalizers.

M N -IFFTs operations inside the IDZT and DZT blocks can be more efficiently implemented. In general, the values of N and M might also play other roles once a specific pilot design and equalization method are selected.

A. Proposed pilot design

In order to relax additional constraints on the parameter M , we propose alternatively the use of Chu sequences [9], which always fulfill the CAZAC property for any length and are defined as

$$\mathbf{a}_p[y] = \begin{cases} e^{j \frac{\pi W}{K} y^2} & \text{if } K \text{ is even} \\ e^{j \frac{\pi W}{K} y(y+1)} & \text{otherwise} \end{cases}$$

where K is the sequence length, W is an integer prime to K and $y \in \{0, \dots, K-1\}$. The proposed pilot configuration, along with the data, is shown on the left side of Fig. 2, where the Chu sequence is placed along one of the columns of the matrix $\mathbf{X}_p^{(s)}$ and it is superimposed with data symbols. For the proposed superimposed pilot (SID) approach we have that

$$\mathbf{X}^{(s)} = \mathbf{X}_p^{(s)} + \mathbf{X}_d^{(s)}$$

where the matrix $\mathbf{X}_d^{(s)} \in \mathbb{C}^{M \times N}$ contains $(M - \ell_M)N$ data symbols in the first $M - \ell_M$ rows. The length of the employed Chu sequence is equal to $M - \ell_M$ to enable the insertion of a pilot CP of length ℓ_M in front of it. This is done to preserve the autocorrelation property of the sequence even after the channel effect and will be formally justified in the last part of this paragraph. Hence, the pilot vector embedded into the matrix $\mathbf{X}_p^{(s)}$ is given as

$$\mathbf{a}_p^{CP} = [\underbrace{a_p[M - 2\ell_M], \dots, a_p[M - \ell_M - 1]}_{\mathbf{a}^{CP}}, \underbrace{a_p[0], \dots, a_p[M - \ell_M - 1]}_{\mathbf{a}_p}]$$

where $\mathbf{a}^{CP} \in \mathbb{C}^{\ell_M}$ is the pilot-CP. We now clarify why adding the CP to the pilot is important. Consider the discrete DD

input-output relation that can be derived by applying the DZT to (6) [14, Chapter 5]

$$\mathbf{Y}[\ell, k] = \sum_{i=1}^P h_i e^{j\frac{2\pi}{MN} k_i (\ell - \ell_i)} \cdot \mathbf{X}[(\ell - \ell_i)_M, (k - k_i)_N] e^{j\frac{2\pi}{N} (k - k_i) \lfloor \frac{\ell - \ell_i}{M} \rfloor}. \quad (11)$$

From (11), we observe that the DD domain is quasi-periodic, i.e., it is periodic up to phase rotations. Each path of the channel scales and shifts the transmitted signal \mathbf{X} along both dimensions according to the complex gains h_i and the DD shifts ℓ_i and k_i . Within every frame, the channel response is completely characterized by the parameters h_i, ℓ_i, k_i , and P . By neglecting for the moment the presence of data symbols and noise, the receiver will only observe P shifted and scaled replicas of the transmitted pilot. When the perfect autocorrelation property of the sequence is fulfilled, one can uniquely identify all the channel parameters by simply checking how many different pilot replicas can be found within the matrix \mathbf{Y} . Recall that, when the CAZAC property is satisfied, the autocorrelation is ideal. Unfortunately, the phase terms in (11) have to be compensated, otherwise the CAZAC property of the pilot is lost. Nevertheless, it can be shown that the only problematic term is $\exp(j\frac{2\pi}{N} (k - k_i) \lfloor \frac{\ell - \ell_i}{M} \rfloor)$, which only affects the first ℓ_M rows of \mathbf{Y} since $\ell_i \leq \ell_M$. Therefore, for channel estimation purposes, we solve this problem at the receiver by considering only the last $(M - \ell_M)$ rows of \mathbf{Y} . Note that, the channel-induced shifts on the transmitted pilot sequence can be seen as circular shifts only when the period of the DD domain along the delay dimension has the same size as the transmitted sequence. However, since at the receiver we are only processing the last $(M - \ell_M)$ rows of the DD matrix, we have to properly select the length of the pilots. Hence, to enforce the periodic behavior of the channel-induced shifts on a period of length $(M - \ell_M)$ we have to introduce the pilot-CP.

We are interested in comparing our pilot construction with what is commonly considered in OTFS literature. Hence, we consider the embedded pilot design of [3] (see Fig. 2)

$$\mathbf{X}^{(e)} = \mathbf{X}_p^{(e)} + \mathbf{X}_d^{(e)}$$

where the matrix $\mathbf{X}_p^{(e)} \in \mathbb{C}^{M \times N}$ contains one unique pilot symbol, and $\mathbf{X}_d^{(e)} \in \mathbb{C}^{M \times N}$ contains data symbols in all positions except the last ℓ_M rows and a rectangle of size $(2\ell_M + 1) \times 2k_M$ centered around the pilot location.

B. Estimation procedure

As in other OTFS studies e.g. [4], [8], channel estimation can be cast as a sparse signal recovery problem

$$\mathbf{y} = \mathbf{\Omega}_p \mathbf{h} + \mathbf{y}_d + \mathbf{w}$$

where $\mathbf{y}, \mathbf{w} \in \mathbb{C}^{NM \times 1}$ are defined in (8) and (9), while the P -sparse vector $\mathbf{h} \in \mathbb{C}^{(L_M+1)2k_M \times 1}$ that models the channel is given as:

$$\begin{cases} \mathbf{h}[\ell_i 2k_M + k_i] = h_i, & \text{if } k_i \geq 0 \\ \mathbf{h}[(\ell_i + 1)2k_M + k_i] = h_i, & \text{if } k_i < 0 \end{cases}.$$

The columns of the matrix $\mathbf{\Omega}_p \in \mathbb{C}^{NM \times (L_M+1)2k_M}$ are

$$\boldsymbol{\omega}_i = (\mathbf{F}_N \otimes \mathbf{I}_M) (e^{-j\frac{2\pi}{NM} k \ell} \mathbf{\Delta}^k \mathbf{\Pi}^\ell) (\mathbf{F}_N^H \otimes \mathbf{I}_M) \mathbf{x}_p \quad (12)$$

for $i \in \{1, 2, \dots, (L_M + 1)2k_M\}$ and $\mathbf{x}_p = \text{vec}(\mathbf{X}_p)$, where \mathbf{X}_p is the DD matrix containing the pilots according to a given design strategy. Each $\boldsymbol{\omega}_i$ is generated using ℓ and k respectively equal to ℓ_i and k_i as in the i -th element of \mathbf{h} . The terms $\mathbf{\Omega}_p \mathbf{h}$ and \mathbf{y}_d represent the contributions on \mathbf{y} of the pilot and the data after being transmitted over the channel. Borrowing the nomenclature of compressed sensing (CS) [15], $\mathbf{\Omega}_p$ is called *sensing matrix*, and can be leveraged at the receiver to estimate the vector \mathbf{h} . Different from standard CS, $\mathbf{\Omega}_p$ cannot be chosen freely as it has to replicate the channel effect and thus the only element we can design is \mathbf{x}_p .

The parameters ℓ_M and k_M are assumed to be known at the transmitter and at the receiver, and can be considered the upper bounds to the channel delay and Doppler spread. The estimation algorithm can exploit the knowledge of these parameters to focus only on the part of the matrix \mathbf{Y} that contains contributions related to the pilot.

When the S1D design presented in Sec. III-A is adopted, the term \mathbf{x}_p in (12) is equal to $\text{vec}(\mathbf{X}_p^{(s)})$, and thus the receiver can discard the first ℓ_M rows of the matrix \mathbf{Y} to perform channel estimation. This operation corresponds to the deletion of some specific rows of $\mathbf{\Omega}_p$. Similarly, when the embedded pilot construction is used we have that $\mathbf{x}_p = \text{vec}(\mathbf{X}_p^{(e)})$ in (12). Also in this case, multiple rows of $\mathbf{\Omega}_p$ can be removed since not all elements of \mathbf{Y} are needed to estimate the channel.

For both pilot constructions, the resulting sensing matrices show a good behavior from a CS point of view since all their columns are independent, implying that the mutual coherence of each of the two matrices is equal to zero. This effect is trivial for the embedded pilot (EP) construction since each column of $\mathbf{\Omega}_p$ will contain only one non zero entry in a different position according to its index. Differently from [8], our S1D pilot design results in a sensing matrix with zero coherence thanks to the ideal autocorrelation properties of the designed sequence. As sparse recovery algorithm we employ orthogonal matching pursuit (OMP) [16]. Note that, given the dimensions of the matrix $\mathbf{\Omega}_p$, the channel estimation problem could also be solved by standard linear methods like zero forcing (ZF) or minimum mean square error (MMSE) but these approaches tend to be complex and yield poorer performance. It is important to highlight that the channel sparsity, i.e., the number of multi-path channel components, is assumed to be unknown in our setting. The stopping condition of the algorithm is therefore modified to accommodate a threshold on the value of the residual. OMP will produce an estimate of \mathbf{h} that we denote as $\hat{\mathbf{h}}$.

C. Equalization and iterative estimation approach

After the execution of the channel estimation procedure, the receiver runs an equalization and demodulation routine to estimate the transmitted data symbols. When data and pilot symbols are non-orthogonal, the pilot contribution has to be

canceled from \mathbf{y} before proceeding with the equalization stage. This operation exploits the channel estimate $\hat{\mathbf{h}}$ as

$$\mathbf{y}'_d = \mathbf{y} - \Omega_p \hat{\mathbf{h}}.$$

The vectors \mathbf{y}'_d and $\hat{\mathbf{x}}_d$ represent the equalizer input and output respectively. We consider as equalizers both the linear minimum mean squared error (LMMSE), which can be derived starting from the input-output relation shown in (11), and the maximal-ratio combining (MRC) from [10]. Both algorithms can be implemented more effectively by leaving ℓ_M empty rows at the bottom of \mathbf{X}_d in the form of zero padding (ZP).²

Depending on the relative power of data and pilots, the performance of any superimposed channel estimation method may be limited by interference due to the data symbols. To mitigate this phenomenon, we could iterate between channel estimation and equalization. Once a first channel estimate is available, the receiver can estimate the data and perform interference cancellation by removing the estimated data combined with the last channel estimate from the original received signal

$$\mathbf{y}'_p = \mathbf{y} - \hat{\Omega}_d \hat{\mathbf{h}}$$

where $\hat{\Omega}_d$ can be generated through (12) by substituting \mathbf{x}_p with $\hat{\mathbf{x}}_d$. At this point, the vector \mathbf{y}'_p is expected to contain a lower interference from data and it is used as input for the channel estimation procedure that will lead to an enhanced estimate of $\hat{\mathbf{h}}$. This procedure can be iterated multiple times.

IV. NUMERICAL RESULTS

In this section, we compare the two pilot constructions and equalization methods presented in Sec. III. We consider a multi-path channel with $\ell_M = 8$, $k_M = 4$ and $P = 5$. Each propagation component has delay and Doppler shifts uniformly generated from the sets $\{0, \dots, \ell_M\}$ and $\{-k_M + 1, \dots, k_M\}$ while the complex gains are $h_i \sim \mathcal{CN}(0, \frac{1}{P})$. The input data symbols are generated from a 4-quadrature amplitude modulation (QAM) constellation and are placed in the OTFS matrix \mathbf{X}_d according to Sec. III-A (see also Fig. 2). The parameters of the transmitter are set to $M = 32$ and $N = 16$. In the following, we define the energy devoted to the pilot signal as *pilot energy*, with the understanding that such energy is concentrated on a single DD symbol in the EP case, and spread over multiple in our proposed S1D case. The total energy budget used for the transmission of each OTFS frame is fixed, so that, when MN equal power symbols are generated with all the available energy, their signal-to-noise ratio (SNR) equals 15 dB. In this setting, we vary the energy split between data and pilot while keeping their sum equal to the total available energy budget. The fraction of energy allocated for the pilot varies between 0.05 and 0.9. The threshold values used as stopping condition for OMP

²As the Doppler spread grows, the EP construction would leave most of the symbols at the bottom of \mathbf{X}_d empty in order to maintain data-pilot orthogonality. In such a case, the cost of introducing the ZP to the full row leading to a better equalization becomes small. To compare the performance of the different channel estimation methods in a fair manner, we then introduce ZP also in our proposed pilot construction S1D.

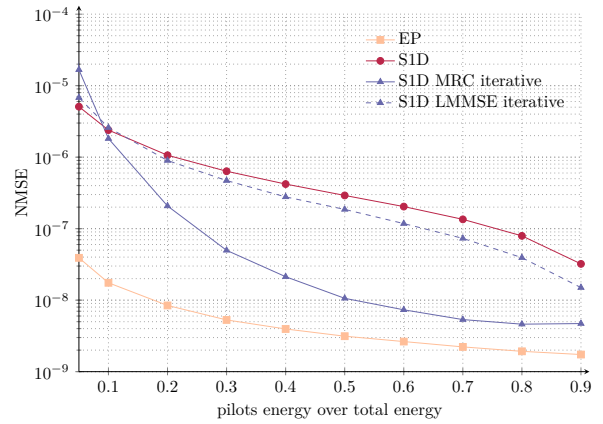


Fig. 3. NMSE of channel estimation as a function of the pilot energy.

are set as 3σ for EP and $3\sigma + P_d$ for S1D, where P_d is the average power of the data symbols. Fig. 3 shows the results for the NMSE, defined as $\frac{\|\hat{\mathbf{H}} - \mathbf{H}\|_2^2}{\|\mathbf{H}\|_2^2}$ where $\hat{\mathbf{H}}$ is the estimated DD channel matrix in the same form of (10) but computed with the estimated channel parameters from $\hat{\mathbf{h}}$. This metric measures the quality of the channel estimate. We note that increasing the pilot symbol energy has a beneficial effect regardless of the pilot construction. For S1D, this effect is amplified as the decrease in energy allocated to data also decreases the interference caused on the pilot sequence. The EP construction achieves the best NMSE across the whole pilots energy range, thanks to data-pilot orthogonality. In order to improve the performance of the S1D method, the iterative detection and demodulation technique described in Sec. III-C is considered, fixing the total number of iterations to 3. The MRC equalizer shows a remarkable improvement when paired with the iterative procedure, and becomes competitive with the EP construction for pilot energy exceeding 0.6. We also note that, for very small pilot energy, the use of the iterative routine may perform worse than the one-shot estimation alone. The reason is that the initial channel estimate may be too imprecise, and causes the incorrect cancellation of data, hence introducing additional interference on the pilot sequence. Finally, for LMMSE the addition of the iterative procedure results in a very limited performance gain. The main reason lies in the difficult task of quantifying the amount of residual interference at each iteration, and thus, it appears difficult to find the right regularization parameter of the equalizer.

Another relevant metric for assessing the pilot construction is the BER. Interestingly, different energy splits have to be chosen to minimize the BER depending on the selected equalizer and pilot design. In general, as shown in Fig. 4, one needs to find the right balance between a good channel estimate (right-end side of the plot) and a sufficiently high SNR for the data symbols (left-end side of the plot). Allocating exceedingly low energy to the pilot degrades the channel estimate, resulting in poor equalization. On the other hand, when too little power is allocated to the data symbols, the system becomes noise-limited. The minimum BER of $\approx 3 \cdot 10^{-4}$ is achieved with

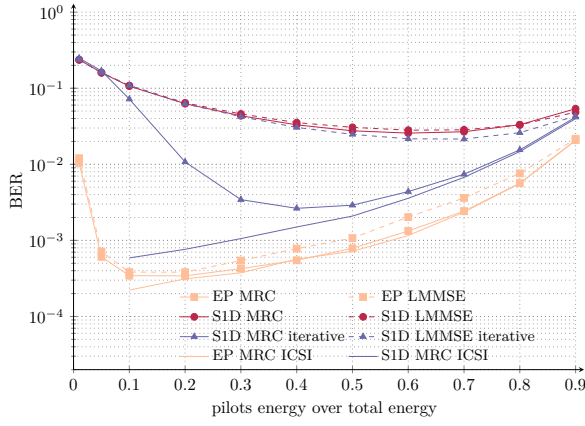


Fig. 4. BER as a function of the pilot energy.

the EP construction, the MRC equalizer and 20% of energy dedicated to the pilot. This result is tightly followed when employing the LMMSE equalizer. The best results achieved with the iterative S1D requires a higher pilot energy (i.e., 40% of the total energy) and the best achieved BER is $\approx 2.5 \cdot 10^{-3}$ when using MRC. The other variants of the S1D construction yield worse performance in terms of BER, as the interference of data negatively impacts the demodulation. In Fig. 4, we also provide the results with ideal channel state information (ICSI) for the different combinations of pilot constructions and equalizers. When sufficient energy is given to the pilots, both the EP and S1D constructions with iterative MRC are very close to the ideal performance. The fact that better BER results are achieved by the EP method reflects the outcome of the NMSE analysis. Indeed, the data-pilot orthogonality enables an interference-free estimation of the channel response that can be leveraged to obtain a better performance of the equalizer. This orthogonality, however, comes at the cost of preventing the full exploitation of the available degrees of freedom in the DD domain, which must remain empty to avoid interference with the pilots and cannot be used for data transmission. When considering the S1D approach, instead, more data symbols can be inserted within each OTFS frame. By doing so, the achievable SE increases drastically. The SE is defined as the average number of successfully decoded information bits per transmitted symbol. Note that, in order to avoid inter-frame interference, a CP that does not add information content is pre-pended to transmitted signal thus increasing the overall length of the frame. This CP penalty is only considered for the S1D construction since for the EP one the presence of the full ZP guard in DD domain already prevents inter-frame interference. The SE results are presented in Fig. 5, where S1D shows a $\approx 57\%$ gain when compared with the EP method. In Fig. 6 we show the results in terms of PAPR. The S1D construction provides the best performance regardless of the pilot energy allocation. With this type of construction, the PAPR is decreasing in function of the pilots energy as the main contribution is given by the data signal. For the EP placement, instead, when most of the energy is allocated to the pilot the PAPR grows very large. It is worth

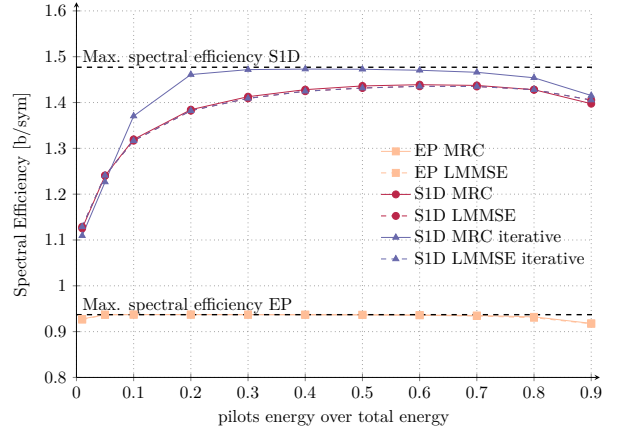


Fig. 5. Average spectral efficiency as a function of the pilot energy.

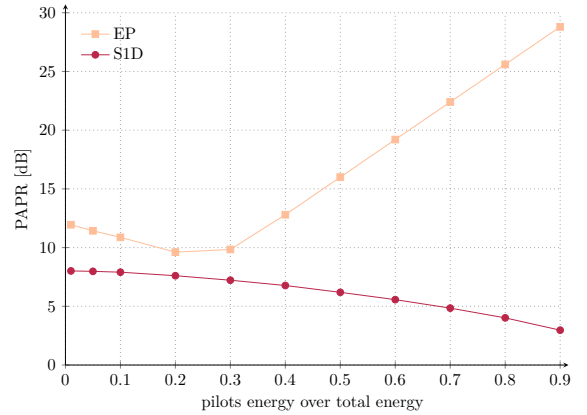


Fig. 6. PAPR as a function of the pilots energy.

noting that the EP construction achieves the best BER and PAPR for the same energy split of 0.2. We leave for future study whether this holds also for other channel models and OTFS frame sizes. Considering the best operating points of both pilot constructions in terms of BER, the use of the S1D method enables a PAPR reduction of ≈ 3 dB.

An apparent result that appears from this case study is that the performance of the communication system has a strong dependency on the selected energy allocation. The intrinsic relationship between performance metrics and the instantaneous parameters (including channel characteristics, noise level, and system numerology) is expected to be non-trivial. In this regard, further research is needed to define a strategy to split the available energy resources a-priori.

From the point of view of complexity, the choice among EP and S1D introduces a possible difference in the cost of executing the OMP algorithm at the receiver side. In particular, the number of rows of the sensing matrix Ω_p for EP and S1D are given as $(\ell_M + 1)2k_M$ and $(M - \ell_M)2k_M$ respectively. When $M \approx \ell_M$ the choice on the pilot constructions does not affect the complexity cost. Note that, since the columns of Ω_p only represent integer DD shifts of the transmitted pilot, for the considered constructions the resulting sensing matrices show ideal coherence properties, meaning that all columns

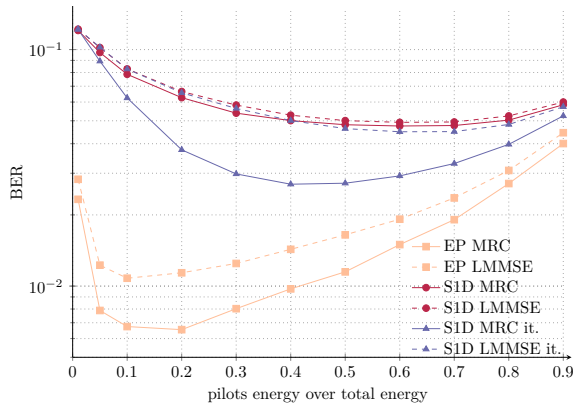


Fig. 7. BER as a function of the pilot energy, with input symbols from the 16-QAM constellation.

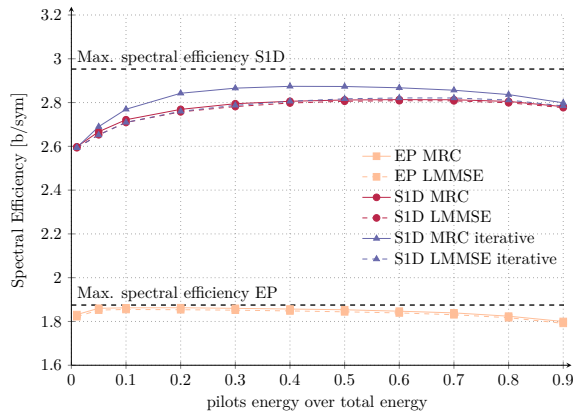


Fig. 8. SE as a function of the pilot energy, with input symbols from 16-QAM constellation.

of Ω_p are linearly independent. In this specific setting, the algorithm OMP can be equally implemented without the need of the least square operation thus avoiding the need of any matrix inversion. Finally, a linear increase in complexity appears when iterative channel estimation and demodulation are employed. In this case, complexity cost is proportional to the number of iterations of interference cancellation.

As a final experiment, we consider the use of 16-QAM to generate the input data symbols. By increasing the modulation order while maintaining the average symbol power fixed, one trades BER for increased SE, as shown in Fig. 7 and Fig. 8. Even when no PAPR requirements are considered, the S1D construction still enables the successful reception of a higher number of bits per OTFS frame. When instead an upper bound on the PAPR is considered, only a small energy split range can be considered to fulfill the requirement. When the PAPR limit is tight, an energy back-off might be necessary and in this latter case, we expect the S1D to better scale given its superiority on this performance criterion.

When the objective is to maximize the SE, the target BER should also be considered. If this requirement allows the use of higher-order modulations for both pilot constructions, then the

proposed S1D method delivers the best performance. However, if the target error probability limits larger constellation sizes only for the superimposed data-pilot construction, the orthogonal EP method should be preferred. Overall, depending on the specific BER and PAPR targets, different data-pilot designs should be chosen to maximize the SE.

V. CONCLUSIONS

In this paper, we proposed a novel superimposed pilot construction for OTFS modulation, designed to improve the SE and lower the PAPR. This construction shows favorable properties when channel estimation is cast as a CS problem. The role of the data-pilot orthogonality in the DD domain is discussed and evaluated via numerical simulations, where we compare the performances of two representative systems. We show that, when iterative estimation and successive cancellation are employed along with our proposed method, a small performance penalty in terms of NMSE of the channel estimate and hence BER can be exchanged for significant gains in terms of PAPR and SE compared to data-orthogonal designs.

REFERENCES

- [1] R. Hadani, S. Rakib, M. Tsatsanis, A. Monk, A. J. Goldsmith, A. F. Molisch, and R. Calderbank, "Orthogonal time frequency space modulation," in *Proc. IEEE WCNC*, 2017, pp. 1–6.
- [2] S. K. Mohammed, R. Hadani, A. Chockalingam, and R. Calderbank, "OTFS—a mathematical foundation for communication and radar sensing in the delay-doppler domain," *IEEE BITS*, vol. 2, no. 2, pp. 36–55, 2022.
- [3] P. Raviteja, K. T. Phan, and Y. Hong, "Embedded pilot-aided channel estimation for OTFS in delay-doppler channels," *IEEE Trans. Veh. Technol.*, vol. 68, no. 5, pp. 4906–4917, 2019.
- [4] W. Shen, L. Dai, J. An, P. Fan, and R. W. Heath, "Channel estimation for orthogonal time frequency space (OTFS) massive mimo," *IEEE Trans. Signal Process.*, vol. 67, no. 16, pp. 4204–4217, 2019.
- [5] Z. Wei, W. Yuan, S. Li, J. Yuan, and D. W. K. Ng, "Off-grid channel estimation with sparse bayesian learning for OTFS systems," *IEEE Trans. Wireless Commun.*, vol. 21, no. 9, pp. 7407–7426, 2022.
- [6] H. B. Mishra, P. Singh, A. K. Prasad, and R. Budhiraja, "OTFS channel estimation and data detection designs with superimposed pilots," *IEEE Trans. Wireless Commun.*, vol. 21, no. 4, pp. 2258–2274, 2022.
- [7] W. Yuan, S. Li, Z. Wei, J. Yuan, and D. W. K. Ng, "Data-aided channel estimation for OTFS systems with a superimposed pilot and data transmission scheme," *IEEE Wireless Commun. Lett.*, vol. 10, no. 9, pp. 1954–1958, 2021.
- [8] Z. Chen, X. Zheng, and X. Chen, "Delay-wise superimposed pilot based compressed sensing channel estimation for OTFS systems," in *Proc. IEEE VTC2023-Fall*, 2023, pp. 1–5.
- [9] D. Chu, "Polyphase codes with good periodic correlation properties (Corresp.)," *IEEE Trans. Inf. Theory*, vol. 18, no. 4, pp. 531–532, 1972.
- [10] T. Thaj, E. Viterbo, and Y. Hong, "General I/O relations and low-complexity universal mrc detection for all OTFS variants," *IEEE Access*, vol. 10, pp. 96 026–96 037, 2022.
- [11] D. Tse and P. Viswanath, *Fundamentals of Wireless Communication*. Cambridge University Press, 2005.
- [12] S. P. S. and A. Farhang, "A practical pilot for channel estimation of OTFS," in *Proc. IEEE ICC*, 2023, pp. 1319–1325.
- [13] J. G. Andrews, "A primer on zadoff chu sequences," *arXiv preprint arXiv:2211.05702*, 2023.
- [14] T. T. Yi Hong and E. Viterbo, *Delay-Doppler Communications Principles and Applications*. Elsevier, 2022.
- [15] Y. C. Eldar and G. Kutyniok, *Compressed Sensing*. Cambridge University Press, 2012.
- [16] Y. Pati, R. Rezaifar, and P. Krishnaprasad, "Orthogonal matching pursuit: recursive function approximation with applications to wavelet decomposition," in *Proc. Asilomar Conf. Sig. Syst. Comput.*, 1993, pp. 40–44 vol.1.